Proceedings of 20th International Congress on Acoustics, ICA 2010

23-27 August 2010, Sydney, Australia

Nonlinear behavior of ultrasound contrast agent microbubbles and why shell buckling matters

Michel Versluis

Physics of Fluids Group and MIRA Institute for Biomedical Technology and Technical Medicine, University of Twente, The Netherlands.

E-mail: m.versluis@utwente.nl

PACS: 43.80.Qf, 43.80.Vj, 43.35.Ei, 43.35.Yb

ABSTRACT

Contrast-enhanced ultrasound imaging relies on the nonlinear scattering of microbubbles suspended in an ultrasound contrast agent. The bubble dynamics is described by a Rayleigh-Plesset-type equation, and the success of harmonic imaging using contrast agents has always been attributed to the nonlinear behavior predicted by this equation. A surfactant layer of phospholipids stabilizes the microbubbles and it has always been assumed that the visco-elastic properties of the coating lead to an increased stiffness and additional damping of the radial dynamics, hence to a reduction of the nonlinear response of the bubbles. Here we show that the coating material in fact leads to an increased nonlinear bubble response even at low acoustic pressures where the traditional models for coated as well as uncoated bubbles would only predict linear behavior. For a selection of bubbles we show a pronounced skewness of the resonance curve for increasing pressures to be the origin of the 'threshold' behavior, where it appears as if the bubbles are activated only at elevated pressures. Another set of bubbles shows a 'compression-only' behavior, where the bubbles are observed to efficiently compress, while their expansion is highly reduced. Moreover, the majority of these bubbles display a very strong subharmonic response. The shell-buckling model by Marmottant *et al.* accounts for buckling and rupture of the shell and captures all of the above cases for a unique set of the shell parameters, the relevant parameter being the phospholipid concentration at the bubble interface.

INTRODUCTION

Ultrasound is the most commonly used medical imaging technique. As compared to computer tomography (CT) and magnetic resonance imaging (MRI) ultrasound offers the advantage that the hardware is relatively inexpensive and that it provides real-time images. Imaging with ultrasound is based on the reflection of the transmitted sound wave at tissue interfaces, where the wave encounters an acoustic impedance mismatch, and scattering due to inhomogeneities in the tissue. Unlike tissue, blood is a poor ultrasound scatterer, resulting in a low contrast echo. To enhance the visibility of the blood pool, ultrasound contrast agents (UCA) have been developed, enabling the visualization of the perfusion of organs. A promising new application of UCA is in molecular imaging [1] with ultrasound and in local drug delivery [2].

The typical UCA is composed of a suspension of microbubbles (radius 1-5 μm) coated with a phospholipid, albumin or polymer shell. The coating decreases the surface tension σ and therefore the capillary pressure $2\sigma/R$ and in addition counteracts diffusion through the interface, thus preventing the bubble from quickly dissolving in the blood. The mechanism by which microbubbles enhance the contrast in ultrasound medical imaging is two-fold. First, microbubbles reflect ultrasound more efficiently than tissue due to the larger difference in acoustic impedance with their surroundings. Second, in response to the oscillating pressure field microbubbles undergo radial oscillations due to their compressibility, which in turn generates a secondary sound wave. The oscillations are highly nonlinear, and likewise the sound emitted by the oscillating bubbles. Several pulse-echo techniques have been developed to increase the contrast-to-tissue ratio (CTR), making use of the nonlinear components in the acoustic response of microbubbles, which are not found in the tissue, e.g. pulse-inversion [3] and power modulation [4]. The nonlinear response specific to coated microbubbles offers the potential for new strategies for the optimization of the CTR.

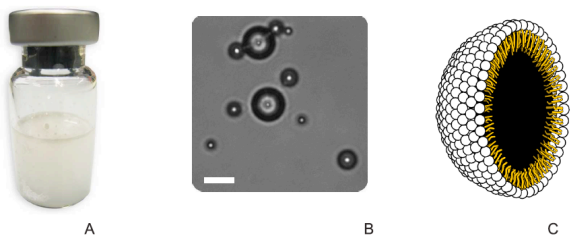

Figure 1. A) Vial containing ultrasound contrast agents. B) Ultrasound contrast agent microbubbles captured in optical microscopy. C) Schematic drawing of a microbubble coated with a phospholipid monolayer

Bubble dynamics modeling

The bubble dynamics in an ultrasound field can be described by a Rayleigh- Plesset type equation [5-7]. The influence of the coating has been investigated in the last two decades, resulting in various extensions of the Rayleigh-Plesset equation. De Jong et al. [8] describe the coating as a thin homogeneous viscoelastic solid with a shell elastic parameter S_p and a shell friction parameter S_f. A more theoretical approach was provided by Church [9] who considered a visco-elastic surface layer of finite thickness. The models by De Jong et al. and Church were both developed for the albumin-coated contrast agent Albunex. Hoff et al. [10] reduced the model developed by Church to the limit of a thin shell. Sarkar et al. [11] proposed a model for a thin shell of a viscoelastic solid where the effective surface tension depends on the area of the bubble and the elasticity of the shell. In the model by Stride [12] the coating is a molecular monolayer, which is treated as a viscoelastic homogeneous material, and the shell parameters depend on the surface molecular concentration. Doinikov et al. [13] addressed the lipid shell as a visco-elastic fluid of finite thickness described by the linear Maxwell constitutive equation. The volumetric oscillations predicted by the Rayleigh-Plesset model can be used to predict attenuation and acoustic backscatter of the agent.

Experimental validation

Experiments on a representative sample of the UCA, containing many microbubbles, confirm the general trends and the influence of the bubble coating as predicted by the models. The resonance frequency is observed to shift to higher frequencies due to the shell stiffness and the extra damping introduced by the shell decreases the overall acoustic response. Van der Meer et al. [14] scanned the insonation frequency at constant acoustic pressure to obtain resonance curves of single bubbles. The acoustic pressure was maintained below 40 kPa to ensure linear bubble dynamics. Van der Meer et al. indeed found an increase of the resonance frequency with respect to uncoated microbubbles.

At a detailed level the agreement between theory and experiment is less convincing. Recent optical characterization studies using high-speed imaging revealed some interesting features of single bubble dynamics that could not be described by the traditional coated bubble models. One of them is “compression-only” behavior reported by de Jong et al. [15], where the bubble oscillations are non-symmetric with respect to the resting radius; the bubbles compress more than they expand. In the study of De Jong et al. `compression-only' behavior was observed in 40 out of 100 experiments on phospholipid-coated bubbles, for acoustic pressures as low as 50 kPa. `Compression-only' behavior was most pronounced for small bubbles. Emmer et al. [16] investigated the nonlinear dynamics of phospholipidcoated microbubbles R_0 = 1-5 μm by increasing the applied acoustic pressure at a constant frequency of 1.7 MHz. They found that a threshold pressure exists, for microbubbles smaller than R_0 = 2 μm, for the onset of bubble oscillations, and that the threshold pressure decreases with increasing bubble size. Bubbles with a radius larger than 2 μm show a linear increase in the amplitude of oscillation with the applied acoustic pressure. Models accounting for a linear viscoelastic shell do not predict the `thresholding' and the `compression-only' behavior.

Shell buckling model

Marmottant et al. [17] developed a model that incorporates the viscoelastic shell and in addition accounts for buckling and rupture of the shell that predicts the `compression-only' behavior in great detail. The model is based on the behavior

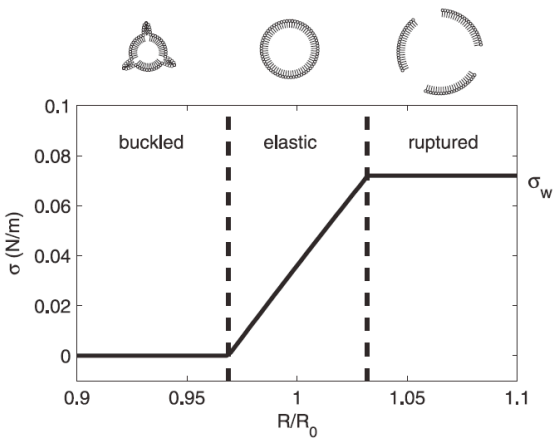

Figure 2. The effective surface tension as a function of the bubble radius (R_0 =2 μm) for the model of Marmottant et al. [12] including an elastic regime and buckling and rupture of the shell.

of a phospholipid monolayer for quasi-static compression [18-20]. Depending on the number of phospholipid molecules per unit area the gas-water interface is shielded to a different extent, resulting in a different effective surface tension. In a small range of expansion and compression the phospholipid-shell behaves elastically as in the previous models and the effective surface tension is linear with the surface area of the bubble. In the elastic regime, compression of the bubble decreases the surface area and assuming a constant number of phospholipids thus increases the packing density and decreases the effective surface tension. For further compression the bubble reaches a critical phospholipid packing density where the dense phospholipid monolayer starts to buckle. Below the buckling radius the effective surface tension vanishes. On the other hand, expansion of the bubble results in a lower packing density. Above a critical radius for the expansion, the concentration of the phospholipids at the interface is so low that the monolayer ruptures. If the gas is in direct contact with the liquid the effective surface tension reaches the surface tension of the water-gas interface, see Fig. 2.

Parameter study

Single bubbles were characterized by scanning in a systematic way one single control parameter. Van der Meer et al. [14] scanned the frequency, resulting in the resonance curve of the bubble. Emmer et al. [16] scanned the driving pressure resulting in the observation of the `thresholding' behavior. While the `thresholding' behavior remained unexplained until now, and it is well known that the resonance curve becomes asymmetrical with increasing acoustic pressure [21, 22], a better insight in the nonlinear phenomena of coated bubbles can possibly be gained from a full parameter study where we scan in a single bubble experiment both the applied acoustic pressure and the insonation frequency.

EXPERIMENTAL

BR-14 (Bracco Research, Geneva) contrast agent microbubbles were injected in an OptiCell chamber (Thermo Fisher Scientific). The chamber was positioned on top of a custom-built water tank. The water tank contained a light fiber and an ultrasound transducer (PA168, Precision Acoustics). A needle hydrophone (HPM02/1, Precision Acoustic) was used to align the ultrasound with the focus of the imaging objective. A XYZ-stage controlled the OptiCell position separately from the watertank in order to keep the ultrasound aligned with the objective. For accurate control of the distance between the bubble and the wall a motorized stage (M-110.2DG, PI) was used.

Figure 3. Optical response of an ultrasound contrast agent microbubble showing 'compression-only' behavior and shell buckling. (R_0 = 3.05 µm, f_{drive} = 1.5 MHz, P_a = 40 kPa, recorded at 14.5 Mfps).

Ultra high-speed imaging

In our optical experiments a high-speed camera was used to record the radial response of single bubbles. Such a camera must temporally resolve the dynamics of the microbubbles driven at MHz frequencies. Therefore framerates of tens of millions of frames per second are required. The Brandaris 128 camera [23] was specifically designed for this purpose. The camera uses a fast rotating mirror (at a maximum of 20,000 rps) to sweep the image across 128 highly sensitive CCDs mounted in a quarter arc. At maximum speed an interframe time of 40 nanoseconds is obtained, which corresponds to a framerate of 25 million frames/s (Mfps). Here the camera was operated at a framing rate near 15 million frames/s. A typical high-speed recording is shown in Fig. 3.

The Brandaris camera was coupled to an optical tweezers setup. A dichroic mirror (CVI) reflected the infrared laser beam (λ = 1064 nm) into the back aperture of the objective (LUMPLFL100xW, Olympus). Individual bubbles were trapped in the low intensity region of a Laguerre-Gaussian beam. The imaging and trapping of the microbubble was performed through the same objective. The dichroic mirror transmitted the visible light used for imaging. Details of the optical tweezers setup coupled to the Brandaris camera can be found in Garbin et al. [24].

Ultrasound

The ultrasound pulses were generated by an arbitrary waveform generator (Tabor Electronics Ltd, Model 8026). The signal was amplified (ENI, Model 350L with 50 Ω input impedance) and sent to the ultrasound transducer. The transducer was calibrated prior to the experiments in a separate water tank over a broad range of frequencies (0.75-5 MHz) and ultrasound pressures. The driving pressure waveform had a length of 10 cycles and the first and last three cycles were apodized with a 3-cycle Gaussian window. In the following we nondimensionalize the driving frequency f with the resonance or Minnaert frequency of the uncoated bubble $f_0^{uncoated}$; $\Omega = f/f_0^{uncoated}$.

Microbubble spectroscopy

The Brandaris ultra high-speed imaging facility can record six movies of 128 frames at up to 25 million frames/s. The camera was designed to also operate in a segmented mode. In practice the conventional single acquisition of 128 frames was replaced by recording two segments of 64 frames each, or four segments of 32 frames each. The camera houses memory space for six conventional acquisitions of 128 frames, before the images are transferred to the PC. Using two segments, this procedure results in the recording of 12 sets of 64 frames. Using four segments has the advantage of an increased frequency resolution, 24 instead of 12, but reduces the sampling of the movies from 64 to 32 frames. The segmented mode allows us to construct a resonance curve of the bubble in a single acquisition, in less than 1 s. The bubble dynamics of the very same bubble was recorded while scanning the applied frequency at constant pressure in each of the 12 movies. The procedure was then repeated for increasing acoustic pressures.

Data analysis

The images from the high-speed movies were analyzed offline with Matlab (The Mathworks, Natick, MA). The radius of the bubble as a function of time R(t) was determined from each image sequence through a semi-automatic minimum cost algorithm [14]. The radius R was normalized to the initial bubble radius R_0. The linear oscillation amplitude A_1 was determined from the individual radius-time curve through filtering with a step function shaped high-pass filter with a cut-off frequency of 1 MHz.

RESULTS AND DISCUSSION

Resonance curves

Fig. 4 shows the resonance curve for three values of the acoustic pressure Pa = 7.5, 12.5, and 25 kPa. The bubble has a radius R_0 = 3.2 µm and is positioned 150 µm from the wall while the applied frequency is between 0.75 and 3 MHz. The experimental data (circles) are compared to the three different models, the uncoated bubble (blue), the coated bubble with a linear viscoelastic shell (black) and the coated bubble including buckling and rupture of the shell (red). To compare the response at the three different acoustic pressures the amplitude of oscillation A_1 is normalized to the maximum simulated response of an uncoated bubble (A_1^{norm}).

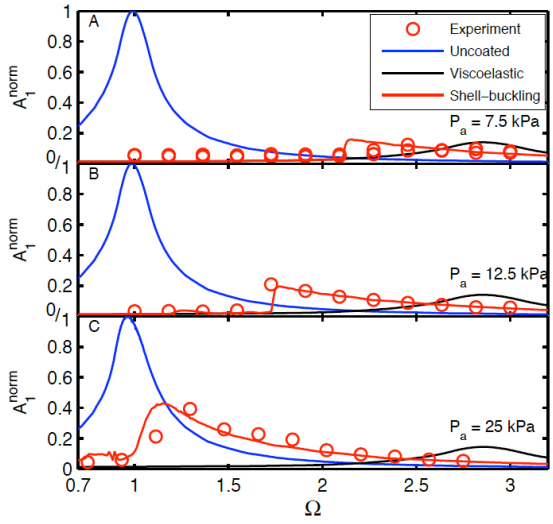

Figure 4. Skewing of the resonance curve of a coated microbubble at low acoustic pressures (Pa = 7.5, 12.5, and 25 kPa). The model for the uncoated bubble (blue) and a linear elastic shell model (black) cannot predict skewing of the resonance curve at low acoustic pressures. The shell model [17] including buckling and rupture (red) captures the skewness of the experimental resonance curve (circles). The bubble radius is 3.2 µm and the shell parameters are the same for both coated bubble models: χ = 2.5 N/m, $\kappa_s = 6 \times 10{-}9$ kg/s and $\sigma(R_0)$ = 0.02 N/m.

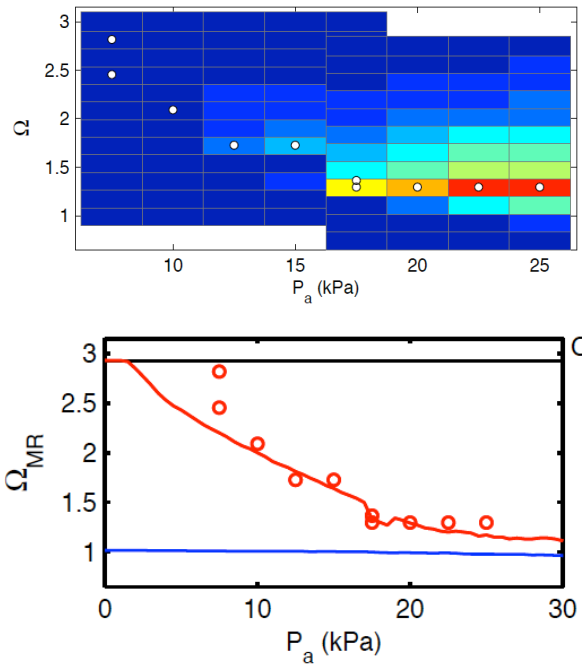

Figure 5. The relative amplitude of oscillations A_1 as a function of the acoustic pressure P_a and frequency Ω. Top: Experimentally measured A_1 as a function of Pa and Ω for a bubble R_0 = 3.2 µm. The frequency of maximumresponse Ω_{MR} (white dots). Bottom: The frequency of maximum response Ω_{MR} as a function of P_a.

For an acoustic pressure P_a = 7.5 kPa (A) the experimental data show a maximum response Ω_{MR} = 2.5. The frequency of maximum response decreases to Ω_{MR} = 1.7 at P_a = 12.5 kPa (B) and to Ω_{MR} = 1.4 at P_a = 25 kPa (C). Besides a decrease in the frequency of maximum response the resonance curves at P_a = 12.5 and 25 kPa are strongly skewed. At low acoustic pressure (P_a = 7.5 kPa) the observed maximum amplitude of oscillation is small compared to the simulated amplitude of an uncoated microbubble A_1^{norm} = 0.1. The maximum amplitude of oscillation increases with increasing acoustic pressure, and for P_a = 25 kPa the normalized amplitude of oscillation is A_1^{norm} = 0.4. The comparison of the experiments with the models showed that the shell-buckling model accounting for an elastic regime, buckling and rupture of the shell (red) captures the decrease in the frequency of maximum response, the asymmetry of the resonance curves, and the relative amplitude of oscillation with a single set of shell parameters.

Full parameter scan

We present the experimentally obtained relative amplitude of oscillation A_1 for the full acoustic pressure and frequency scan in an iso-contour plot in Fig. 5 (top). A total of 120 R(t)-curves have been measured near the frequency of maximum response Ω_{MR} in the acoustic pressure range Pa = 7.5 to 25 kPa at an interval of 2.5 kPa. Fig. 6 shows the simulations with the shell-buckling model with the same shell parameters as in Fig. 5. The experimental frequency of maximum response Ω_{MR} obtained from Fig. 5 (top) (circles) is compared with simulations for the three different models in Fig. 5 (bottom). Ω_{MR} decreases by 50% for an increase of the acoustic pressure from Pa = 7.5 to Pa = 25 kPa. The frequency of maximum response Ω_{MR} simulated with the shell-buckling model (red) is in excellent agreement with the experimental results. For comparison the frequency of maximum response obtained with the model for an uncoated bubble and the

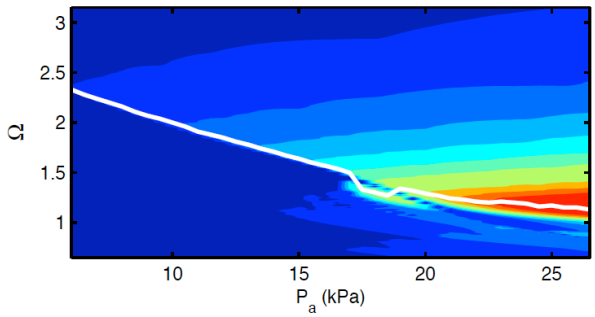

Figure 6. Simulations with the model including buckling and rupture of the shell. The white line shows the frequency of maximum response Ω_{MR}. The bubble has a radius of 3.2 µm and the values for the shell parameters are χ = 2.5 N/m, κ_s = 6 × 10−9 kg/s and σ (R_0) = 0.02 N/m.

linear viscoelastic model are shown. In the shell-buckling model at low acoustic pressures Pa < 2 kPa the oscillations are in the elastic regime and the frequency of maximum response equals the resonance frequency of a coated bubble that follows from the linear viscoelastic model. Above acoustic pressures Pa > 2 kPa the shell starts to buckle and the frequency of maximum response decreases rapidly, approaching the resonance frequency of an uncoated bubble at Pa > 20 kPa.

Origin of the 'thresholding' behavior

A vertical scan line of Fig. 5 (top) and 6 results in the typical resonance curves shown in Fig. 4. A horizontal scan line on the other hand results in the pressure-dependent response for different applied frequencies. De facto this is the same experiment as performed by Emmer et al. [16] with the exception that Emmer et al. varied bubble radius R_0, not the frequency. Such a horizontal scan-line is depicted in Fig. 7 where the relative amplitude of oscillation A_1 is shown for three applied frequencies Ω = 2.1, Ω = 1.5, and Ω = 1. For each frequency, the experimentally observed amplitude of oscillations (circles) increases nonlinearly with increasing acoustic pressure. In particular, the so-called `thresholding' behavior is apparent. The threshold pressure for the onset of oscillations depends on the frequency and is most pronounced for Ω = 1.5, where the bubble shows no oscillations if driven below P_a = 15 kPa and abruptly starts to oscillate (A_1 = 0.1) at P_a = 17.5 kPa. The shell-buckling model (solid lines) reproduces the data accurately and predicts the `thresholding' behavior.

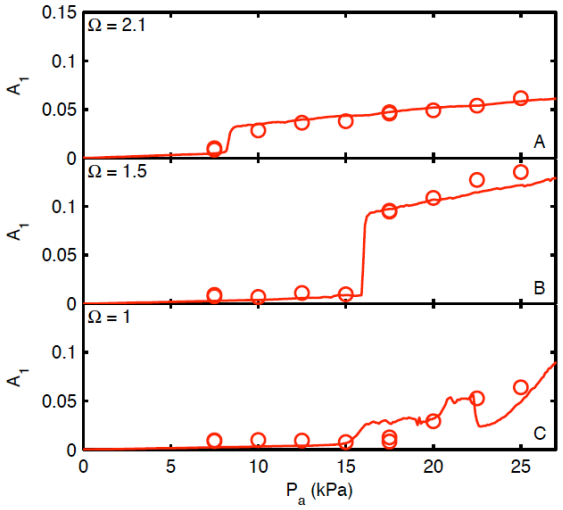

Figure 7. Relative amplitude of oscillation A_1 as a function of the acoustic pressure P_a.

Initial state of the bubble

The decrease of the resonance frequency with increasing pressure as shown in Fig. 5 (bottom) does not uniquely describe the response of all bubbles. We observe a different behavior for different bubbles, even for bubbles of the same size. Fig. 8 shows the frequency of maximum response Ω_{MR} of two equally sized bubbles R_0 = 2.4 μm. To allow for a comparison of the response of different bubbles we plot Ω_{MR} as a function of A_1 instead of P_a. One bubble has a frequency of maximum response Ω_{MR} = 2.2 at A_1 = 0.03 and shows a decrease in the frequency of maximum response of 40% with increasing A_1, reaching a value of Ω_{MR} = 1.4 at A_1 = 0.12 (triangles). The second bubble shows very different behavior, Ω_{MR} = 1.4 and independent of A_1 (squares).

The experimental results are compared to calculations of the frequency of maximum response simulated with the shell-buckling model. The simulations indicated that different values of the shell parameters χ and κ_s show that these parameters do not change the observed trend in Ω_{MR} with A_1. Therefore simulations were performed with only one single free parameter, the initial phospholipid concentration expressed in the effective surface tension at rest $\sigma(R_0)$. The shell elasticity χ was taken 2.5 N/m and the shell viscosity κ_s was 6×10^{-9} kg/s. Fig. 8 shows that the way the frequency of maximum response changes with the amplitude of oscillation is well captured with two extreme values of the effective surface tension. Simulations for a bubble initially in the elastic state, $\sigma(R_0) = \sigma_w/2$ (red), capture the strong decrease in Ω_{MR} (triangles), while simulations for a bubble initially in the buckled state, $\sigma(R_0)$ = 0 N/m (blue), describe the observed constant frequency of maximum response with increasing oscillation amplitude (squares).

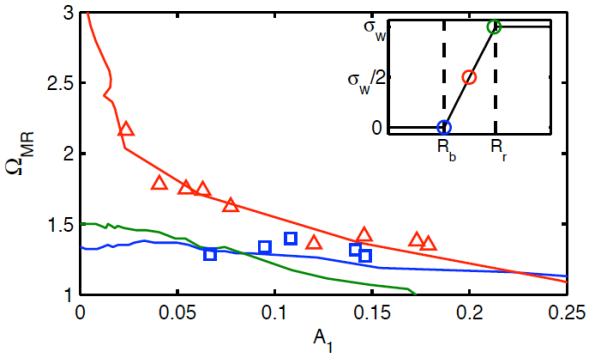

Figure 8. Normalized frequency of maximumresponse Ω_{MR} as a function of the relative amplitude of oscillation A1 for two equally sized microbubbles R_0 = 2.4 μm. One of the bubbles shows a decrease in the frequency of maximum response Ω_{MR} (triangles), while the other bubble has a constant frequency of maximum response (squares). Simulations are shown with the shell-buckling model for three initial cases: the bubble is initially in the buckled state (blue), the ruptured state (green), and the elastic regime (red), see inset. The shell elasticity and shell viscosity are respectively, χ = 2.5 N/m, $\kappa_s = 6 \times 10^{-9}$ kg/s.

CONCLUSIONS

We investigated experimentally the influence of the phospholipid coating on the dynamics of ultrasound contrast agent microbubbles. We recorded the radial dynamics of individual microbubbles with an ultra-high speed camera as a function of the driving pressure and frequency. We observed a strong nonlinear contribution of the coating on the dynamics in agreement with previous experimental observations. These include the "thresholding" behavior, 'compression-only' behavior. The phospholipid coating was found to enhance the nonlinear bubble response at acoustic pressures as low as 5 kPa. For increasing acoustic pressures a decrease of the frequency of maximum response was observed for a distinct class of bubbles, leading to a pronounced skewness of the resonance curve, which we showed to be the origin of the "thresholding" behavior. For other bubbles the frequency of maximum response was found to lie just above the resonance frequency of an uncoated microbubble, and to be independent of the applied acoustic pressure. The shell-buckling bubble model by Marmottant et al., which accounts for buckling and rupture of the shell, captures both cases for a single value of the shell elasticity and shell viscosity. The difference in the observed nonlinear dynamics between the two sets of bubbles can be explained by a difference in the initial surface tension, which is directly related to the phospholipid concentration at the bubble interface. A bubble oscillating in the elastic regime shows "thresholding" behavior and is specifically beneficial for power modulation imaging. A bubble with an initial radius that equals the buckling radius shows "compression-only" behavior. We found that a small change in the initial bubble radius is sufficient to change the initial surface tension, leading to a dramatic change of the observed behavior. As the shell-buckling model describes the dynamics of phospholipid coated bubbles in great detail the model allows for an optimization of current pulse-echo techniques and for the development of new pulse-echo techniques.

ACKNOWLEDGMENTS

This work is part of the PhD thesis of Marlies Overvelde (University of Twente, 2010) and has been made possible by the numerous scientific contributions of the ultrasound contrast agent microbubble teams of the University of Twente (Detlef Lohse, Sascha Hilgenfeldt, Philippe Marmottant, Sander van der Meer, Jeroen Sijl, Benjamin Dollet, Marlies Overvelde, Valeria Garbin, Todd Hay) and Erasmus MC Rotterdam (Nico de Jong, Ton van der Steen, Ayache Bouakaz, Chien Ting Chin, Dave Goertz, Marcia Emmer, Rik Vos) and by financial contributions of the Foundation for Fundamental Research on Matter FOM, the Interuniversity Cardiology Institute of the Netherlands ICIN, the Technology Foundation STW, University of Twente Spearhead Research Programme on Non-Invasive Molecular Tumor Imaging and Killing NIMTIK, Innovation Subsidy of SenterNovem on Bubbles for Ultrasound and Therapy BURST, Bio-sensors for Diagnosis and Healthcare Specific Targeted Research Project of the European Commission on Targeted Microbubbles and Remote Ultrasound Transduction TAMIRUT, The Netherlands Organisation for Scientific Research NWO Rubicon Fellowship, Acoustical of Society of America ASA Hunt Fellowship. BR-14 ultrasound contrast agent bubbles were kindly provided by Bracco Research, Geneva, Switzerland.

REFERENCES

1 J.R. Lindner, "Microbubbles in medical imaging: current applications and future directions" *Nat. Rev. Drug Discov.* **3**, pp. 527–533 (2004)

2 A.L. Klibanov, "Microbubble Contrast Agents: Targeted ultrasound imaging and ultrasound-assisted drug-delivery applications" *Invest. Radiol.* **41**(3), pp. 354–362 (2006)

3 D. Hope Simpson, C.T. Chin, and P.N. Burns, "Pulse inversion doppler: a new method for detecting nonlinear echoes from microbubble contrast agents" *IEEE Trans. Ultrason. Ferroelec. Freq. Contr.* **46**(2), pp. 372–382 (1999)

4 G.A. Brock-Fisher, M.D. Poland, and P.G. Rafter, "Means for increasing sensitivity in non-linear ultrasound imaging systems" US patent no. 5577505 (1996)

5 M.S. Plesset and A. Prosperetti, "Cavitation and bubble dynamics" *Ann. Rev. Fluid Mech.* **9**(1), pp. 145–185 (1977)

6 T.G. Leighton, *The Acoustic Bubble* (Academic Press, 1994). ISBN 0124419208

7 M.P. Brenner, S. Hilgenfeldt, and D. Lohse, "Single-bubble sonoluminescence" *Rev. Mod. Phys.* **74**(2), pp. 425–484 (2002)

8 N. de Jong, R. Cornet, and C.T. Lancée, "Higher harmonics of vibrating gas-filled microspheres. Part one: simulations" *Ultrasonics* **32**(6), pp. 447–453 (1994)

9 C.C. Church, "The effects of an elastic solid surface layer on the radial pulsations of gas bubbles" *J. Acoust. Soc. Am.* **97**(3), pp. 1510–1521 (1995)

10 L. Hoff, P. C. Sontum, and J. M. Hovem, "Oscillations of polymeric microbubbles: Effect of the encapsulating shell" *J. Acoust. Soc. Am.* **107**(4), pp. 2272–2280 (2000)

11 K. Sarkar, W.T. Shi, D. Chatterjee, and F. Forsberg, "Characterization of ultrasound contrast microbubbles using in vitro experiments and viscous and viscoelastic interface models for encapsulation" *J. Acoust. Soc. Am.* **118**(1), pp. 539–550 (2005)

12 E. Stride, "The influence of surface adsorption on microbubble dynamics" *Phil. Trans. R. Soc. A* **366**, pp. 2103–2115 (2008)

13 A.A. Doinikov and P.A. Dayton, "Maxwell rheological model for lipidshelled ultrasound microbubble contrast agents" *J. Acoust. Soc. Am.* **121**(6), pp. 3331–3340 (2007)

14 S.M. van der Meer, B. Dollet, C. T. Chin, A. Bouakaz, M. Voormolen, N. de Jong, M. Versluis, and D. Lohse, "Microbubble spectroscopy of ultrasound contrast agents" *J. Acoust. Soc. Am.* **121**(1), pp. 648–656 (2007)

15 N. de Jong, M. Emmer, C.T. Chin, A. Bouakaz, F. Mastik, D. Lohse, and M. Versluis, "'Compression-only' behavior of phospholipid-coated contrast bubbles" *Ultrasound Med. Biol.* **33**(4), pp. 653–656 (2007)

16 M. Emmer, A. Van Wamel, D. E. Goertz, and N. de Jong, "The onset of microbubble vibration" *Ultrasound Med. Biol.* **33**(6), pp. 941–949 (2007)

17 P. Marmottant, S.M. van der Meer, M. Emmer, M. Versluis, N. de Jong, S. Hilgenfeldt, and D. Lohse, "A model for large amplitude oscillations of coated bubbles accounting for buckling and rupture" *J. Acoust. Soc. Am.* **118**(6), pp. 3499–3505 (2005)

18 J.M. Crane and S.B. Hall, "Rapid compression transforms interfacial monolayers of pulmonary surfactant" *Biophys. J.* **80**(4), pp. 1863–1872 (2001)

19 M.A. Borden and M.L. Longo, "Dissolution behavior of lipid monolayercoated, air-filled microbubbles: Effect of lipid hydrophobic chain length" *Langmuir* **18**(24), pp. 9225–9233 (2002)

20 L. Pocivavsek, R. Dellsy, A. Kern, S. Johnson, B. Lin, K.Y.C. Lee, and E. Cerda, "Stress and fold localization in thin elastic membranes" *Science* **320**(5878), pp. 912–916 (2008)

21 A. Prosperetti, "Nonlinear oscillations of gas bubbles in liquids: transient solutions and the connection between subharmonic signal and cavitation" *J. Acoust. Soc. Am.* **57**(4), pp. 810–821 (1975)

22 W. Lauterborn, "Numerical investigation of nonlinear oscillations of gas bubbles in liquids" *J. Acoust. Soc. Am.* **59**(2), pp. 283–293 (1976)

23 C.T. Chin, C. Lancée, J. Borsboom, F. Mastik, M.E. Frijlink, N. de Jong, M. Versluis, and D. Lohse, "Brandaris 128: A digital 25 million frames per second camera with 128 highly sensitive frames" *Rev. Sci. Instr.* **74**(12), pp. 5026–5034 (2003)

24 V. Garbin, D. Cojoc, E. Ferrari, E. Di Fabrizio, M.L.J. Overvelde, S.M. van der Meer, N. de Jong, D. Lohse, and M. Versluis, "Changes in microbubble dynamics near a boundary revealed by combined optical micromanipulation and high-speed imaging" *Appl. Phys. Lett.* **90**, p. 114103 (2007)